Global contraction of Antarctic Bottom Water between the 1980s and 2000s[*]

SARAH G. PURKEY[1,2,3] and GREGORY C. JOHNSON[2,1]

[1]*School of Oceanography, University of Washington, Seattle WA 98195, USA*

[2]*NOAA/Pacific Marine Environmental Laboratory, Seattle WA 98115, USA*

for *Journal of Climate*

submitted 20 October 2011

revised 19 January 2012

[*] Pacific Marine Environmental Laboratory Contribution Number 3771

[3]*Corresponding author address*: Sarah G. Purkey, School of Oceanography, Box 357940, University of Washington, Seattle WA 98195-7940, USA. E-mail: sarah.purkey@noaa.gov.

ABSTRACT

A statistically significant reduction in Antarctic Bottom Water (AABW) volume is quantified between the 1980s and 2000s within the Southern Ocean and along the bottom-most, southern branches of the Meridional Overturning Circulation (MOC). AABW has warmed globally during that time, contributing roughly 10% of the recent total ocean heat uptake. This warming implies a global-scale contraction of AABW. Rates of change in AABW-related circulation are estimated in most of the world's deep ocean basins by finding average rates of volume loss or gain below cold, deep potential temperature (θ) surfaces using all available repeated hydrographic sections. The Southern Ocean is losing water below $\theta = 0$°C at a rate of -8.2 (±2.6) × 10^6 m^3 s^{-1}. This bottom water contraction causes a descent of potential isotherms throughout much of the water column until a near-surface recovery, apparently through a southward surge of Circumpolar Deep Water from the north. To the north, smaller losses of bottom waters are seen along three of the four main northward outflow routes of AABW. Volume and heat budgets below deep, cold θ surfaces within the Brazil and Pacific basins are not in steady state. The observed changes in volume and heat of the coldest waters within these basins could be accounted for by small decreases to the volume transport or small increases to θ of their inflows, or fractional increases in deep mixing. The budget calculations and global contraction pattern are consistent with a global scale slowdown of the bottom, southern limb of the MOC.

1. Introduction

The Meridional Overturning Circulation (MOC) may play a significant role in climate change (e.g., Meehl et al. 2006) and the deep ocean plays a significant role in ocean heat storage (Levitus et al. 2005; Purkey and Johnson 2010). The strength of the MOC determines the ability of the deep ocean to absorb and store anthropogenic heat and carbon (e.g., Sigman and Boyle 2000; Russell et al. 2006). While the MOC has often been considered to be in steady state in recent decades, rates of deep and bottom water production and circulation were dramatically different during the Last Glacial Maximum, and changes in the MOC have been linked to periods of rapid climate change (e.g., Clark et al. 2002; Lynch-Stieglitz et al. 2007). Models suggest the MOC will slow under global warming scenarios, possibly producing large regional variations in surface temperatures (Solomon et al. 2007). Furthermore, climate models differ widely in their projections of how much heat the deep ocean will absorb under global warming, causing a large spread in future climate projections (Boe et al. 2009).

Cold, dense water formed at high latitudes feeds the deep and bottom limbs of the MOC (Lumpkin and Speer 2007). North Atlantic Deep Water (NADW) is a combination of water masses formed in the Labrador and the Nordic seas (LeBel et al. 2008). NADW travels south at depth until it enters the Antarctic Circumpolar Current (ACC) and rises, as seen by the distinct signature of warm salty water at mid- and upper depths (Orsi et al. 1995; Johnson 2008). In the southern hemisphere, the densest bottom water, Antarctic Bottom Water (AABW), that underlies NADW is also a mixture of water masses, and is formed in at least three locations along the Antarctic shelf (Orsi et al. 1999). At each location, physical mechanisms including ice formation, surface cooling, and mixing with

54 ambient water as it cascades down the continental slope (Foster and Carmack 1976)
55 create a distinct variety of AABW. Each AABW variety enters the lower ACC, further
56 mixing with overlying water, and leaves the Southern Ocean as a slightly less dense
57 water mass (Orsi et al. 1999), here still referred to as AABW. AABW flows north, filling
58 the deepest portions of the Pacific, Indian, and western Atlantic oceans (Johnson 2008).
59 The bottom, southern limb of the MOC transports roughly 20 Sv (1 Sv = 1×10^6 m^3
60 s^{-1}) northward out of the Southern Ocean (Lumpkin and Speer 2007), primarily in four
61 deep western boundary currents (DWBCs; Fig. 1). Chlorofluorocarbon-11 (CFC-11)
62 inventories confirm that true AABW and other warmer, lighter water masses formed in
63 the Southern Ocean contribute about 21 Sv to this MOC limb (Orsi et al. 2002). Inverse
64 models estimate northward transports of AABW into the Pacific, Atlantic, and Indian
65 oceans from 7–11, 5–6, and 8–10 Sv, respectively, although definitions of AABW
66 density and the location of the Southern Ocean boundary vary slightly among studies
67 (Ganachaud and Wunsch 2000; Sloyan and Rintoul 2001; Lumpkin and Speer 2007).
68 Velocity measurements within DWBCs along the Kerguelen Plateau in the Indian Ocean
69 and north of the Falkland Plateau in the Atlantic Ocean imply northward transports of ~8
70 Sv of water for $\theta \leq 0.2$°C in each, but with high temporal variability (Whitworth et al.
71 1991; Fukamachi et al. 2010). In the Pacific, velocity measurements at 32°S have shown
72 the DWBC to transport 15.8 (±9.2) Sv of bottom and deep waters, mostly of southern
73 origin, northward (Whitworth et al. 1999).
74 Numerous studies have shown that the Southern Ocean has warmed significantly
75 throughout the water column. The upper 1000 m of the Southern Ocean has warmed
76 faster than the upper ocean global mean rate between the 1950s and 2000s (Gille 2002;

77 2008; Böning et al. 2008). Below 1000 m, the deep ocean has warmed by ~0.03°C
78 decade^{-1} south of the Subantarctic Front between the 1980s and 2000s (Purkey and
79 Johnson 2010). In addition, previous studies have shown property changes in AABW
80 and its components near its source regions. In the Weddell Gyre, Warm Deep Water
81 (WDW), Weddell Sea Deep Water (WSDW), and Weddell Sea Bottom Water (WSBW)
82 have all exhibited warming trends since 1990, although, more recently, WDW has
83 fluctuated between warming and cooling (Robertson et al. 2002; Fahrbach et al. 2004;
84 2011). In addition, glacier melt has freshened shelf water near the deep-water formation
85 regions in the Weddell Sea (Hellmer et al. 2011). In the Ross Sea, shelf water and
86 bottom water have freshened over the past 50 years (Jacobs and Comiso 1997; Jacobs and
87 Giulivi 2010). Finally, bottom waters off the Adelie Coast have cooled and freshened on
88 isopycnals between the mid-1990s and mid-2000s (Aoki et al. 2005; Rintoul 2007;
89 Johnson et al. 2008a; Jacobs and Giulivi 2010).
90 Warming of AABW has also occurred along its spreading paths outside of the
91 Southern Ocean (Purkey and Johnson 2010; Kouketsu et al. 2011). Regional studies
92 within the Scotia Sea, Brazil Basin, Argentine Basin, Australian-Antarctic Basin, Pacific
93 Basin, and Southwest Pacific Basin have all shown significant warming of AABW over
94 the past few decades (Coles et al. 1996; Fukasawa et al. 2004; Johnson and Doney 2006;
95 Kawano et al. 2006; Johnson et al. 2007; Zenk and Morozov 2007; Johnson et al. 2008a;
96 Meredith et al. 2008; Kawano et al. 2010). On average, the deep ocean below 4000 m
97 has absorbed ~0.03 W m^{-2} (expressed as a flux over the entire surface area of Earth)
98 between the 1980s and 2000s with stronger warming near the source regions (Purkey and
99 Johnson 2010). The deep ocean heat uptake, which is often neglected in heat and sea

100 level rise budgets, is important in quantifying Earth's net energy imbalance (e.g., Willis
101 et al. 2008; Church et al. 2011). In climate models, periods of decreased upper ocean
102 heat uptake (and pauses in global average surface warming) are characterized by
103 increases in deep ocean heat uptake (Meehl et al. 2011), further emphasizing the
104 importance of accurately quantifying total ocean heat uptake, not just the upper few
105 hundred meters.

106 It is difficult to quantify past effects of global warming on the MOC strength directly
107 owing to a lack of the data needed to determine its historical strength and natural
108 variability (Kanzow et al. 2007). Using data from multiple occupations of a single zonal
109 hydrographic section across the North Atlantic, Bryden et al. (2005) found a 30%
110 reduction in the upper, northern limb of the MOC from 1957 to 2003. However, mooring
111 array data later showed short-term variability to be larger than the previously reported
112 long-term trend from the temporally sparse section data, calling the previous results into
113 question (Cunningham et al. 2007). Using the western halves of most of the occupations
114 of this same section, a decrease in transport in the bottom, southern limb of the MOC
115 carrying AABW northward into the North Atlantic has been reported from 1983 to 2003
116 (Johnson et al. 2008b), with evidence of a partial rebound in 2010 (Frajka-Williams et al.
117 2011). While this limb of the MOC may exhibit less temporal variability so far from its
118 source, these transport estimates were still made using geostrophic shear and relying
119 upon an inferred level of no motion. Similarly, a decreasing trend in northward bottom
120 water transport across 24°N in the Pacific has been suggested between 1985 and 2005
121 (Kouketsu et al. 2009).

However, deep warming signals on pressure surfaces also imply deepening potential isotherms – changes in the vertical distribution of water masses through the water column (Kouketsu et al. 2009; 2011; Masuda et al. 2010). These changes have been attributed to a decrease in bottom water export from the Southern Ocean into deep ocean basins (Masuda et al. 2010; Kouketsu et al. 2011) and thus could be a signal of a slowdown in the bottom limb of the MOC. Indeed, Kouketsu et al. (2011) found decreases in northward flowing water below 3500 m across 35°S in the Pacific and western Atlantic between the 1990s and 2000s in a data assimilation that includes the deep warming signals.

Here we estimate changes in the bottom, southern limb of the MOC globally using 32 repeated oceanographic sections (hereafter sections), with a total of 145 occupations between 1981 and 2011, by calculating the increase or decrease in volume below multiple deep potential temperature (θ) surfaces. The sections are grouped within and averaged over each measured deep ocean basin. We use the rates of change in volumes of these cold, dense waters to infer changes in the deep and bottom circulation. While the difference of a section occupied twice may still be subject to short-term variability, the calculation of rates, often over multiple occupations, together with the estimation of means from multiple sections within a basin, usually creates a statistically significant result. This technique allows more robust estimates of changes in the MOC than those derived from geostrophic transport estimates across a single transoceanic hydrographic section.

2. Data

144 The data used for this study are from an assembly of 32 full-depth, high-quality, ship-
145 based hydrographic sections that have been occupied two or more times between 1981
146 and 2011 (Fig. 1). The data set is comprised of the publicly available conductivity-
147 temperature-depth (CTD) instrument data on http://cchdo.ucsd.edu/ as of September
148 2011, collected either through the World Ocean Circulation Experiment (WOCE)
149 hydrographic program or the GO-SHIP program in support of the Climate Variability
150 (CLIVAR) and carbon cycle science programs. Data along sections were collected at
151 stations nominally spaced at 55 km. Each station includes a vertical profile of
152 temperature, salinity, and pressure from the surface to a depth of 10–20 m from the
153 bottom. Accuracy of temperature, salinity, and pressure are nominally 0.002°C, 0.002
154 PSS-78, and 3 dbar respectively (Joyce 1991). Most of the deep ocean basins are crossed
155 by at least one section (Fig. 1). The time and number of occupations varies among
156 sections, but the mean time difference between the first and last occupation for all
157 sections considered here is 14.5 years with the mean first occupation occurring in 1991
158 and the mean last in 2006. For the three southernmost basins (Fig. 1), the mean time
159 difference is 13.9 years with the mean first occupation in 1993 and the mean last in 2006.
160 Prior to analysis, the data are screened so only data with good quality flags are used. In
161 addition, only occupations deemed sufficiently close (in space) to prior occupations along
162 a given section are used (see Purkey and Johnson 2010 for details).
163 A full description of the temporal and spatial distribution of the bulk of data used here
164 can be found in Purkey and Johnson (2010). Four new sections and seven new
165 occupations of previously used sections have become available since the publication of
166 Purkey and Johnson (2010) and are added to the data set they used for this analysis. The

new sections, identified by their WOCE designators, include: P09 running along 137°E between 10°N and 30°N with occupations in 1994 and 2010, S4P running along 67°S between 170°E and 70°W occupied in 1992 and 2011, SR01 running along 65°W between 57°S and 63°S occupied in 1993, 1994, 1996, and 1997, and I02/IR06 running roughly along 8°S between 94°E and 106°E and then diagonally between 9°S, 106°E to 24°S, 111°E occupied in 1995 and 2000 (Fig. 1). Additional occupations of existing sections previously used include: the 1983 occupations of A20 and A22, the 2005 occupation of A12, the 1992 and 2005 occupation of SR04, the 2008 occupation of SR03, and the 2011 partial occupation of A16. All new sections are screened and gridded for use following Purkey and Johnson (2010).

3. Volumetric rate of change analysis

Along many sections, a visible rising or sinking of potential isotherms can be observed between occupations, especially in the Southern Ocean (e.g., Fig. 2). Except within temperature inversions, areas of sinking isotherms are correlated with areas of warming on isobars (and areas of rising with cooling). Similarly, the sinking of an isotherm within a basin implies a loss of water below that θ (Fig. 2), and the rising implies a gain. For example, both occupations of a meridional section across the Australian-Antarctic Basin reveal cold AABW cascading down the continental shelf into the deep ocean on the southern side of the basin (Fig. 2a). However, the coldest deep isotherms ($\theta \leq$ -0.2°C) across this basin systematically fall with time between occupations, implying a volumetric loss of these deep and bottom waters. By θ = 0.2°C the isotherms are centered around similar depths for both occupations, implying an

189 increase with time in the volume of water within $-0.2 \leq \theta \leq 0.2$°C that compensates for
190 the contraction of the coldest waters near the bottom, at least in this particular section.
191 To quantify the loss or gain of water as a function of θ, we first calculate the depth of
192 the isotherms for each occupation along each section. We analyze 811 θ surfaces,
193 referred to as the θ grid, ranging from -2.2°C to 32°C with a spacing of 0.01°C below
194 3°C and a spacing of 0.1°C above 3°C. For each occupation at each location along a
195 section, the θ-pressure profile is converted to a θ-depth profile and linearly interpolated
196 onto the θ grid. Any θ inversions starting from the bottom up are masked over; in other
197 words, the depth of each θ is defined as the deepest depth at which that θ is found. This
198 convention means that upper water column θ minimums (inversions) are not included in
199 this analysis.
200 The sections are apportioned to the 33 deep basins they cross. The basin boundaries
201 follow the bottom topography and are mostly isolated by at least the 3000 m isobath
202 (Fig.1; Smith and Sandwell 1997). The basin boundaries are those used in Purkey and
203 Johnson (2010) except that their Amundsen-Bellingshausen Basin (ABB) has been
204 subdivided into the ABB and the Scotia Sea here (Fig. 1). Most of the major deep ocean
205 basins are crossed by at least one repeat section (Fig. 1), with the exceptions of the
206 Arabian Sea and Somali Basin, where no repeat sections are available owing to recent
207 piracy-related safety concerns.
208 Along each section, within a given basin, the mean rate of change in height above the
209 bottom ($\overline{\partial h / \partial t}$), its standard deviation ($\sigma_{\partial h/\partial t}$), and total degrees of freedom (DOF) are
210 calculated for all values of the θ grid. The height (h) is the difference between the
211 potential isotherm depth (d_i) and that of the sea floor (d_b; Smith and Sandwell 1997; Fig.

212 3a). The quantity $\partial h/\partial t$ is found from the slope of a least-squares linear fit of the
213 isotherm heights to their dates of occupation (e.g., Fig 3b). The DOF are computed as the
214 horizontal length of the section sampled for $\partial h/\partial t$ for a given isotherm divided by a
215 horizontal decorrelation scale for deep ocean θ of 163 km estimated by Purkey and
216 Johnson (2010). Sampled regions isolated by topography over a distance less than the
217 decorrelation length scale and separated from adjacent sampled regions by distances
218 more than the decorrelation length scale are assumed to be statistically independent and
219 add one DOF.

220 Two screening criteria are applied to mask out regions with insufficient spatial or
221 temporal coverage. First, if the time between the first and last occupation is less than 2.5
222 years, $\partial h/\partial t$ is discarded. Second, if the sum of the area covered by a given θ along a
223 section is less than 111 km, $\overline{\partial h/\partial t}$ is not used. Isotherms sampled for less than 111 km
224 are likely based on data from two or fewer CTD stations, making their mean depth
225 unreliable. This criterion eliminates the coldest, deepest isotherms in many basins (such
226 as the coldest AABW water cascading down over the Antarctic continental shelf and
227 slope), but it ensures that we are looking at robust, basin-scale means, which are the focus
228 of this paper.

229 The $\overline{\partial h/\partial t}$, $\sigma_{\partial h/\partial t}$, and DOF along all sections within a given basin are used to compute
230 the basin-mean $\overline{\partial h/\partial t}$, $\overline{\partial h/\partial t}_{bsn}$, and its uncertainty for each θ value. If there is only one
231 section crossing the basin, the $\overline{\partial h/\partial t}$ for that section is assumed to represent the whole
232 basin. If there are multiple sections crossing a given basin, a length-weighted average is
233 found using the horizontal length occupied by each θ on each section as its weight. The
234 standard error is calculated by dividing the standard deviation by the square root of the

DOF, and then a length-weighted average of the standard errors are found. The total DOF for the basin is the sum of the DOF associated with each θ for all sections within the basin. In addition to the basin variability, the 3 dbar and 0.002ºC measurement accuracy of the CTD pressure and temperature sensors translate to a 12 m uncertainty at most in isotherm depths for any given cruise. This instrumental uncertainty is neglected hereafter because it is very small compared to that arising from natural variability (e.g., Fig 2).

Finally, the $\overline{\partial h/\partial t}_{bsn}$ is scaled to a rate of change in volume (ΔV) within the basin using climatological data (Gouretski and Koltermann 2004; e.g., Fig 3c). The climatological data set has a half-degree horizontal resolution with 45 depths. At each location θ is calculated from salinity, temperature, and depth data. Each profile is interpolated onto a 20 m vertical grid using a piecewise cubic Hermite interpolation and linearly interpolated onto the θ grid following the same method described above. The climatological data are divided into the 33 basins. For each basin, the total surface area covered by each θ is calculated. The $\overline{\partial h/\partial t}_{bsn}$ and associated standard error for each basin and θ are converted to ΔV within that basin by multiplying by the corresponding climatological surface area. Two-sided 95% confidence intervals are estimated from Student's t-distribution using the standard errors and total DOF.

The result is a profile of ΔV versus θ with 95% confidence intervals for each of the 27 basins with data (e.g., Fig. 4). Negative values of ΔV indicate a contraction of water below the associated potential isotherm, zero indicates no change, and positive indicates net gain. When water is lost between successively warmer isotherms, the ΔV curves have a negative slope. Vertical portions of the curves indicate no additional loss of water between isotherms, but also no recovery. A positive slope indicates an increase in the

amount of water between successively warmer isotherms. The error estimate reflects both the variability across sections and the number of data points. If a given θ is not well sampled, its associated error will be large. The surface area of each isotherm scales both its ΔV and the associated error. For example, the 95% confidence interval around the WEB ΔV curve (Fig. 4a) narrows with increasing depth (decreasing θ) since the total basin volume below a given isotherm decreases with decreasing temperature. In contrast, the $\overline{\partial h / \partial t}_{bsn}$ and associated error for the WEB does not (Fig. 5).

4. Southernmost basin changes

The ΔV profiles of the three southernmost basins (Fig. 1) all show a remarkably similar pattern (Fig. 4; orange curves). Each reveals a loss of volume, ranging from -1.6 to -3.6 Sv, within the coldest ~0.5°C of the water column and a recovery from the bottom water contraction within the θ classes of the Circumpolar Deep Water (CDW).

In the Weddell-Enderby Basin (WEB; Fig. 1) of the South Atlantic Ocean, a contraction of bottom water is found for $\theta < -0.55$°C, with a maximum value of -3.6 (±2.0) Sv (Fig. 4a). This rate of change in volume is equivalent to a mean isotherm fall rate of ~15 m yr^{-1} (not shown). Within error bars, this maximum value of ΔV aligns with the -0.7°C boundary between WSBW and WSDW (Carmack and Foster 1975; Orsi et al. 1993) and is found roughly 1000–2000 m above the bottom of the basin. Above the WSBW, we find no significant gain or loss of WSDW for $-0.7 < \theta < 0$°C (Fig. 4a). The bottom water contraction is compensated higher in the water column by an increase in the volume of water with $0.25 < \theta < 0.5$°C. This water is found shallower than 1000 m, where a tongue of lower CDW rises to the south in the ACC as it enters the basin from

280 the north. The ΔV curve for the basin suggests a southward surge of CDW into the
281 region.

282 Is there a discernible regional pattern of AABW contraction within the WEB? The
283 WEB ΔV curve contains data from three sections: The zonal section SR04 cutting across
284 the Weddell Gyre at approximately 65°S, the meridional section A12 running along the
285 Greenwich Meridian, and the meridional section I06 running along 30°E (Fig. 1). That
286 all three sections show a negative $\partial h/\partial t$ for $\theta < 0$°C and overlap among their 95%
287 confidence intervals indicates an overall consistency of vertical isotherm motions across
288 the basin (Fig. 5). Error is reduced in the mean compared to the individual sections
289 owing to the increase in DOF.

290 Bumps and wiggles in the mean curves have to be considered in the context of their
291 associated uncertainties. Most sections in the southern basins exhibit a large contraction
292 of water in their coldest temperature class, causing a negative bulge in the mean curve at
293 that potential temperature. The location of the section determines this value and it does
294 not necessarily represent the overall volume rate of change of the basin. The bulge at $\theta =$
295 -0.82°C in the WEB (Figs. 4 and 5) is an example. This bulge is not outside the
296 confidence limits of the rates given for the θs above and below (Fig. 4). Thus the θ of
297 maximum volume loss in each basin effectively has uncertainties determined by the
298 confidence intervals for ΔV around that θ. For example, above we assert $\theta =$ -0.55°C
299 exhibits maximum volume loss within the WEB. But because the contraction rate at $\theta =$
300 -0.55°C is somewhere between 5.8 and 1.8 Sv, this is only an estimate of the isotherm –
301 at 95% confidence the real value lies somewhere from $0.6 > \theta > -0.7$°C (Fig. 4a).

The Australian-Antarctic Basin of the South Indian Ocean (Fig. 1), fed by both WSBW and Adelie Land Bottom Water (ALBW; Mantyla and Reid 1995), shows a loss of -2.2 (±1.1) Sv of water with $\theta < 0$°C (Fig. 4b), equivalent to a mean isotherm fall rate of 14 m yr^{-1}. The mean ΔV curve does not show a full recovery from the bottom water contraction until $\theta = 2.5$°C, although the curve is not significantly different from zero for $\theta \geq 0.5$°C. These increasing volumes of warmer temperatures suggest a surge of upper CDW from the north is replacing the bottom water losses.

In the ABB of the South Pacific Ocean (Fig. 1), a maximum loss of -1.1 (±0.3) Sv of water colder than 0°C is found (Fig. 4c), equivalent to a mean fall rate of 13 m yr^{-1}, a pattern similar to that for the Australian-Antarctic Basin (Fig. 4b). Water colder than 0°C is within the temperature range of AABW produced in the Ross Sea. It is known as Ross Sea Bottom Water (RSBW), and previously characterized by salinities > 34.7 and $\theta <$ 0°C (Jacobs et al. 1970). The ABB exhibits a more diffuse recovery from the bottom water contraction than the WEB; in the former the ΔV curve increases slowly between 0 and 1.5°C. Water with $\theta \sim 1.5$°C is upper CDW, found around 1000 m depth in the ABB. Our results suggest an influx of upper CDW from the north in the ABB.

5. Changes along the northward paths of AABW

AABW spreads north, primarily along four main DWBCs, out of the Southern Ocean (Fig. 1), filling the bottom-most reaches of most of the world's deep basins (Johnson 2008; Lumpkin and Speer 2007). The Southern Ocean retains a large reservoir of AABW (Fig. 6) as deep ridges restrict its northward transport, their sills limiting the density (and cold temperature) of water that continues north (Orsi et al. 1999; Johnson 2008). The temperature of outflowing waters should be warmed by the observed descent

325 of isotherms in the southern basins, provided they fall at sills. The ΔV curves reveal a
326 clear pattern of decreased AABW volume transport to the north along three of the four
327 main DWBCs leaving the Southern Ocean (Fig. 4). In each case, the θ class below which
328 the contraction is observed increases to the north due to mixing along the path and,
329 presumably, isotherms sinking with time at the sills (Fig. 4).

330 In the West Atlantic, the basins directly to the north of the WEB along the DWBC of
331 AABW show a volume loss within the AABW (Fig. 4a). Water as cold as θ = -0.6°C
332 leaves the WEB (Fig.6; Gouretski and Koltermann 2004) and flows into both the Scotia
333 Sea and the Argentine Basin (Meredith et al. 2008) although extensive volumes of cold
334 water within these basins do not start until around -0.2°C (Gouretski and Koltermann
335 2004). In the WEB a 10 m yr^{-1} isotherm descent rate is observed below -0.2°C. Along
336 the north ridge of the WEB, the vertical θ gradient is about 0.1°C in 300 m, suggesting
337 the outflowing water should have warmed by roughly 0.07°C over the past ~20 years.
338 This hypothesis is supported by the ΔV curves in the Scotia Sea and Argentine Basin to
339 the north.

340 The Scotia Sea exhibits at most a small and highly uncertain volume loss of -0.4
341 (±2.1) Sv below 0.2°C. The Scotia Sea is crossed by two meridional sections: A16 and
342 S01. A16 shows a large ~30 m yr^{-1} descent of isotherms between -0.5 and 0.5°C,
343 consistent with the isotherm descent observed in the WEB. However, S01, located
344 farther to the west, shows a rising of isotherms but with an extremely large uncertainty.
345 As a result, the mean (not shown) shows no significant volume loss or gain at any
346 potential temperature. Although no statistically significant trend was found in our

347 analysis, Meredith et al. (2008) reported a decrease in volume of water colder than 0°C in
348 the Scotia Sea between 1995 and 2005 in the A16 data.

349 Cold water from both the Scotia Sea and directly from the WEB feed the Argentine
350 Basin (Fig. 1; Meredith et al. 2008). A maximum bottom water contraction of -2.2 (±2.1)
351 Sv of water below -0.2°C is observed there (Fig 4a, green curve) equivalent to an
352 isotherm fall rate of ~15 m yr^{-1}, again consistent with observations in the WEB. The first
353 isotherm to span the width of the basin fully is θ = -0.2°C. Between -0.2°C and the
354 coldest sampled water, a small volume loss is observed (Fig. 4). Colder than -0.2°C,
355 isotherms cascade downward on the south side of the basin, and thus only cover a small
356 volume of water. These waters may be undersampled here. We do not quantify volume
357 changes for θ < -0.4°C because there are either no data or insufficient data. A full
358 recovery from the bottom water contraction appears to occur by ~ 2°, although for θ >
359 -0.15°C the volume changes are no longer significantly different from zero (Fig. 4a).
360 South of the equator, a strong deep thermocline for 1 < θ < 2°C denotes the vertical
361 interface between the north flowing AABW and the south flowing NADW above (e.g.,
362 Johnson and Doney 2006). The ΔV pattern indicates that the AABW contraction may be
363 compensated by an increase in NADW in the Argentine Basin.

364 Farther to the north, in the Brazil Basin (Fig. 1), we again find significant loss of the
365 deepest, coldest northward flowing bottom waters. The coldest water to exit the
366 Argentine Basin into the Brazil Basin is θ ~ 0.2°C, but again, the bottom of the basin is
367 filled with warmer waters, around 0.3°C. Here, a loss of -0.6 (±0.3) Sv (or a mean
368 isotherm fall rate of 9 m yr^{-1}) for waters colder than 0.3°C is observed in the deepest
369 water. The contraction continues to a maximum loss of -0.8 (±0.3) Sv for waters below

370 0.86°C (Fig. 4a, purple curve) and does not fully recover until above 2°C, again near the
371 upper extent of AABW influence (e.g., Johnson and Doney 2006).
372 In the west Indian Ocean DWBC (Fig. 1), bottom water flows out of the WEB into
373 the Crozet Basin, followed by the Madagascar Basin, Somali Basin, and Arabian Sea
374 (e.g., Mantyla and Reid 1995; Sloyan 2006). While this DWBC is fed by the same
375 source water as the northward flowing western Atlantic DWBC, there are no statistically
376 significant cold θ depth changes along this path outside of the WEB, possibly due to a
377 lack of data (Fig. 1). Changes in this DWBC system are not discussed further here.
378 In the east Indian Ocean, water above 0.5°C flows north out of the Australian-
379 Antarctic Basin into the South Australian Basin through the Australian-Antarctic
380 Discordance (Fig. 1; e.g., Sloyan 2006). Colder than 0.5°C, a descent rate of -10 (±16) m
381 yr^{-1} is observed in the Australian-Antarctic Basin, suggesting about a 0.1°C increase in
382 the coldest bottom water leaving the Australian-Antarctic Basin, given the vertical
383 temperature gradient near the basin's northern boundary. The South Australian Basin
384 shows a slight loss of ~ -0.3 Sv of water colder than 0.7°C, but it is not significantly
385 different from zero (Fig. 4b). Any possible contraction is recovered by 1.2°C and with a
386 continued positive slope the basin shows a net gain in water by 1.7°C. The uncertainties
387 for the ΔV curve in this basin are large, and none of these results are significant at the
388 95% confidence level.
389 The Wharton Basin (Fig. 1), however, does show a statistically significant loss of
390 bottom water (Fig. 4b). About 4.4–5.8 Sv of water colder than 0.64°C flows out of the
391 South Australian Basin into the Wharton Basin through a gap between the Broken and
392 Naturaliste plateaus (Sloyan 2006). We find a small but statistically significant

393 contraction of -0.1 (±0.05) Sv below this θ value in the Wharton Basin, which shows a
394 maximum decrease of -0.75 (±0.4) Sv at 0.8°C, again corresponding to the coldest waters
395 to span the whole basin. This bottom water contraction slowly recovers between 0.8 and
396 1.3°C. AABW-derived waters in the Wharton Basin cross the Mid-Indian Ridge into the
397 Mid-Indian Basin (Warren and Johnson 2002), but we find no significant trend of cold
398 bottom water volumes in the Mid-Indian Basin (not shown).
399 In the Pacific, water from both the Australian-Antarctic Basin and ABB feed the
400 DWBC that flows northward through the Southwest Pacific Basin (Fig. 1; Whitworth et
401 al. 1999). The coldest water to enter the Southwest Pacific Basin has $\theta \sim 0.4$°C, and
402 there is a substantial volume in the basin below 0.6°C. The Australian-Antarctic Basin
403 and ABB show an isotherm fall rate between 3 and 6 m yr^{-1} below 0.6°C. Subsequently,
404 the Southwest Pacific Basin ΔV profile shows loss of -5 (±4.5) Sv of the coldest
405 measured water at 0.54°C (Fig. 4c). Above the large bottom water loss, the isotherms
406 between 0.57 and 0.62 all descend by ~12 m yr^{-1}, causing a continued significant
407 contraction rate of ~2 Sv which is recovered by around 1°C.
408 The northward flow of bottom water continues into the Pacific Basin (Fig. 1) through
409 the Samoan Passage with deep northward flow estimated at 10.6 (±1.7) Sv below θ =
410 1.1°C and 4.8 (±0.3) Sv below 0.8°C (Roemmich et al. 1996). Here we find a
411 statistically significant reduction of -3.4 (±1.4) Sv below 1.1°C and a small change of ~
412 -0.1 Sv below 0.8°C (Fig. 4c). Above 1.1°C there is a slight recovery, but the curve stays
413 statistically significantly negative, with an isotherm decent of ~ 0.5 m yr^{-1} until 5°C.

414 **6. Basin budgets**

In steady state, maintenance of the vertical θ structure in abyssal basins can be modeled as a balance among the lateral inflow of cold AABW, geothermal heating at the sea floor, vertical mixing with warmer water above, and vertical advection (upwelling). However, the ΔV curves imply that heat and volume budgets below deep, cold θ surfaces are not in steady state in many deep basins. We diagnose these departures from steady state with volume and heat budgets for the Pacific Basin below $\theta = 1$ °C and the Brazil Basin below 0.8 °C and determine how inflowing AABW transport or θ, geothermal heating, or vertical mixing would have to change in order to account for the observed volume and heat changes. We chose these examples because accurate temperature and volume transport estimates are available for these basins below isotherms at which we find significant ΔVs.

Observed ΔVs imply ~15% imbalances in the deep basin volume budgets. Morris et al. (2001) estimate the net lateral inflow of water (through several channels) of $\theta < 0.8$ °C into the Brazil Basin at 3.70 Sv from current meter data, dominated by a 4.02 Sv inflow through the Vema Channel. Steady-state volume balance would require upwelling at a rate of 3.70 Sv through $\theta = 0.8$ °C. However, the observed ΔV of 0.56 Sv at $\theta = 0.80$ °C (Fig. 4a), requires a 14% reduction of inflow through the Vema Channel to 3.46 Sv or a 15% increase in upwelling to 4.26 Sv. Similarly, Roemmich et al. (1996) found 11.22 Sv of inflow for $\theta < 1$ °C into the Pacific Basin through the Samoa Passage and environs. With no lateral outflow of water for $\theta < 1$ °C, upwelling through this surface must also be 11.22 Sv in steady state. The observed ΔV of 1.98 Sv at $\theta = 1$ °C (Fig. 4c), requires a 18% reduction of inflow or increase of upwelling.

437 The extent to which the observed ΔV changes perturb the steady-state heat budget
438 can be diagnosed following Morris et al. (2001). By assuming steady state conservation
439 of volume and heat below cold, deep potential isotherms in the Brazil Basin, Morris et al.
440 (2001) estimated vertical diffusion coefficients. We start with a slightly modified steady-
441 state equation (see Table 1) that balances lateral transports and upwelling of heat, vertical
442 mixing of heat, and geothermal heating at the sea floor.
443 An imbalance term, the rate of change in heat storage (Table 1, rightmost
444 column), is calculated from the ΔV curves (Fig. 4) below select isotherms (θ_{top}). Since
445 the ΔV curves are cumulative sums over θ intervals they are first differentiated with
446 respect to θ, multiplied by θ_{top} - θ (since water must be heated to θ_{top} before exiting the
447 control volume), and then integrated from the bottom up to θ_{top}. In both the Pacific and
448 Brazil basins the time-dependent heat storage terms are not negligible compared to the
449 dominant terms in the steady-state budget. In the Pacific Basin, the heat storage term is
450 ~6% of the advective or mixing terms and comparable to the geothermal term (Table 1).
451 In the Brazil Basin, the heat storage term is about 8% of the advective or mixing terms
452 and about four times higher than the geothermal term (Table 1).
453 We diagnose the changes in water volume transports through deep passages (U_i),
454 transport-weighted potential temperatures of $U_i(\theta_i)$, κ, θ_z, or Q (Table 1) required to
455 account for the observed changes in heat storage below θ_{top} in the Brazil and Pacific
456 basins. These estimates all assume a new steady-state balance has been reached. First, Q
457 would have to almost double in the Pacific Basin and more than quintuple in the Brazil
458 Basin to account for the observed changes in heat storage. We know of no evidence or
459 plausible reason that such a change in geothermal heating has occurred.

460 In both basin budgets, the heat storage term is about 6 to 8% of the advective and
461 mixing terms. Hence, for the Pacific Basin, U_i at the Samoa Passage would have to
462 decrease by 0.65 Sv below 1 °C , from 11.22 to 10.57 Sv, to account for the change in
463 heat storage. For the Brazil Basin, U_i in the Vema Channel would have to decrease by
464 0.33 Sv below 0.8 °C, from 4.02 to 3.69 Sv. Both changes are less than those required to
465 balance volume. Alternatively, θ_i in the Samoa Passage would have to increase by 0.013
466 °C, from 0.77 to 0.78 °C, a plausibly small amount. In the Brazil Basin, θ_i through the
467 Vema Channel would have to warm by 0.06 °C, from 0.03 to 0.09 °C, broadly consistent
468 with an observed 0.03 °C decade^{-1} increase in the coldest θ in that channel over recent
469 decades (Zenk and Morozov 2007).
470 Changes in κ or θ_z required to account for the observed changes in heat storage (Table
471 1) are equally small. For the Pacific Basin κ would have to increase from 5.63 to 5.98 ×
472 10^{-4} m^2 s^{-1} or θ_z from 0.28 to 0.30 × 10^{-3} °C m^{-1}. In the Brazil Basin, κ would have to
473 increase from 4.34 to 4.70 × 10^{-4} m^2 s^{-1} or θ_z from 1.41 to 1.53 × 10^{-3} °C m^{-1} to account
474 for the change in heat storage. Such undetectably small changes cannot be ruled out.
475 However, θ_z increases would be unexpected, since warming bottom waters should
476 decrease θ_z.

477 **7. Discussion**

478 Here we have shown a large decrease of the volume of AABW over time in the
479 Southern Ocean, consistent with a slowdown of the bottom, southern limb of the MOC.
480 Classically defined AABW ($\theta \leq 0$°C) is largely limited to the Australian-Antarctic Basin,
481 ABB, WEB, Argentine Basin, Scotia Sea, and Agulhas-Mozambique Basin. In these
482 basins, $\theta = 0$°C has fallen at a rate of -13.2 (±6.7), -11.4 (±2.9), -8.1 (±4.5), -9.5 (±9.6),

483 -8.6 (±40.3), and -6.4 (±12.1) m yr^{-1}, respectively. The area-scaled sum of these rates
484 yields an estimated contraction rate of -8.2 (±2.6) Sv for water colder than 0°C (Table 2).
485 To the north, along the three best-sampled paths for exporting AABW-derived bottom
486 waters from the Southern Ocean in the lower limb of the MOC, we find a smaller
487 contraction of the volume of the coldest, deepest water. These volume losses suggest a
488 global slowdown of the bottom limb of the MOC. Ventilation timescales along the
489 bottom limb of the MOC from the Southern Ocean to the abyssal north Pacific are of
490 order 1000 years (e.g., DeVries and Primeau 2011), much longer than the timescales of
491 this study. However, previous studies have demonstrated that a reduction of AABW
492 formation around Antarctica can be communicated through the abyss in just decades by
493 planetary waves (e.g., Masuda et al. 2010). Budget calculations in two well-measured
494 deep basins suggest that the observed bottom water temperature trends could be owing to
495 a change in the transport of bottom water entering the basin.
496 These results hinge on the assumption that the data analyzed are representative of the
497 deep sampled basins both spatially and temporally over the past 30 years. The spatial
498 coverage of the data appears generally good, with most basins analyzed having repeat
499 sections crossing them at roughly even distances, especially in the Southern Ocean (Figs.
500 1 and 6). This assumption of spatial representativeness can be checked by comparing the
501 isotherm height rates of change ($\partial h/\partial t$) [Eq. (1)] along all sections within basins with
502 multiple crossings. For example, in the WEB, the portions of three sections crossing that
503 basin all show a similar pattern and amplitude in their $\partial h/\partial t$ curves (Fig. 5). On average,
504 isotherms within the WSBW have a descent rate of -22.5 (±21.6) and -11.5 (±13.4) m yr^{-1}
505 along A12 and SR04, respectively (Fig. 5). Within the WSDW, A12, SR04, and I06

506 exhibit average isotherm descent rates of -3.8 (±7.1), -9.4 (±4.8), and -16.5 (±12.9) m
507 yr^{-1}, respectively (Fig. 5). Given the location of the sections (Figs. 1 and 6) and their
508 relatively uniform patterns of isotherm descents (Fig. 5), it seems unlikely that the
509 volume of the coldest waters has remained constant and instead has shifted around this
510 basin due to changes in gyre strength or location, as suggested previously (Fahrbach et al.
511 2011). Furthermore, when the ΔV curves for this basin and many others are calculated
512 with different subsamples of the sections crossing those basins, there usually are only
513 small variations in the curves.
514 Second, here we assume that the temporal data coverage is sufficient to capture any
515 trend. For sections with more than two occupations, this assumption usually appears
516 valid (e.g., Fig. 2b). Although looking for geostrophic transport trends in multiple
517 occupations of a single section can be misleading because variations in a few stations can
518 dominate such a calculation (e.g., Cunningham et al. 2007), here all the station data from
519 multiple occupations of multiple sections are being averaged over very large areas. This
520 procedure should reduce smaller scale temporal or spatial noise. Furthermore, our error
521 analysis quantifies the variability within our data set. In most of the basins presented
522 here, results are statistically significantly different from zero, which suggests that these
523 results are more robust than previous studies of multiple occupations of a single section.
524 A slowdown of the AABW production rate is consistent with the freshening of shelf
525 waters in AABW formation regions in the Ross and Weddell seas in recent decades (Aoki
526 et al. 2005; Jacobs and Giulivi 2010; Hellmer et al. 2011). The surface freshening
527 increases the stability of the water column, making it more difficult for surface waters to
528 sink, possibly causing a slowing of the bottom limb of the MOC (Stouffer et al. 2007). In

529 the Ross Sea, the shelf water and RSBW have freshened by ~0.03 and ~0.01 decade^{-1},
530 respectively, between 1958 and 2008 (Jacobs and Giulivi 2010), most likely caused by
531 recent glacial melt along the Amundsen and Bellingshausen seas freshening the westward
532 flowing coastal current (Rignot et al. 2008; Jacobs and Giulivi 2010). Along the coast at
533 140ºE and within the central Australian-Antarctic Basin, AABW has also warmed and
534 freshened (Aoki et al. 2005; Johnson et al. 2008a), again pointing toward a freshening of
535 the shelf water end member of either, or both, RSBW and ALBW. In the Weddell Sea,
536 the northwestern shelf water has freshened by 0.09 between 1989 and 2006, owing to
537 increasing glacial melt water input, changes in sea ice extent, and higher precipitation
538 (Hellmer et al. 2011).

539 The recent positive trend in the Southern Annular Mode (SAM) has been connected
540 directly and indirectly to AABW formation rates. Due to past ozone depletion, the
541 summer time SAM index has been trending positive since the 1950s and is predicted to
542 continue positive due to global warming (Thompson et al. 2011). A positive trend in the
543 SAM is associated with stronger and more poleward westerly winds over the Southern
544 Ocean (Gillett and Thompson 2003; Arblaster and Meehl 2006; Thompson et al. 2011)
545 and southward migration of the ACC with associated warming (Gille 2008). Even
546 though the SAM trend is only significant during the summer months and AABW is
547 formed during winter, SAM changes may contribute to increased glacial melt, a
548 southward shift in the ACC, warmer temperatures, and increased precipitation over the
549 Southern Ocean. Given the timescales involved with these phenomena, summer SAM
550 changes could be linked to the observed slowdown of AABW. Further, models have
551 shown the strengthening and the southward migration of westerlies is tied to a net

552 increased of inflow of NADW into the South Atlantic (e.g., Oke and England 2004) and
553 an increase in the northward Ekman transport, which leads to a strengthening of CDW
554 upwelling (e.g., Russell et al. 2006), consistent with our results. Finally, models have
555 also demonstrated that SAM variability can lead to changes in ice formation and melting
556 connected directly to bottom water formation (Gordon et al. 2007; Klinger and Cruz
557 2009; Kirkman and Bitz 2011).

558 In addition to a slowdown in AABW formation rates, shifts in other physical
559 processes could also have contributed to the observed AABW volume loss. First,
560 geothermal heating could have increased and warmed AABW. We have no reason to
561 believe geothermal heating in the Southern Ocean has increased dramatically in the past
562 several decades. In more northerly basins, Q would have to increase unrealistically in
563 order to account for observed heat storage changes (Section 6).

564 Second, one might argue that the same amount of AABW is being produced, but is
565 now warmer and fresher, hence lighter. As noted above, shelf water components of
566 AABW have freshened in recent decades, linked to freshening of ALBW and RSBW
567 (Aoki et al. 2005; Jacobs and Giulivi 2010). In addition, the shelf water entrains adjacent
568 waters as it descends the continental slope to form AABW. Therefore, recently reported
569 warming of adjacent water masses such as CDW (e.g., Böning et al. 2008) or changes in
570 entrainment rates could also affect AABW properties. Indeed, a southward surge of
571 CDW to replace the reduction in AABW, suggested by our calculations, could affect
572 AABW properties. However, if the AABW changes were in its properties and not its
573 formation rate, the ΔV curves in the southernmost basins would exhibit a sharp negative
574 spike centered around the change in θ of the AABW, which is not observed (Fig. 4).

575 Third, a small change in mixing rates could produce a basin-wide deep warming (e.g.,
576 Section 6). However, we know of no reason to believe mixing rates have changed over
577 recent decades. Of course, if AABW formation rates have slowed, AABW residence
578 times within these basins could increase, at least while the system adjusts, allowing more
579 time for AABW to mix with overlying waters even if the mixing coefficient does not
580 change. In this respect, the rates of AABW volume changes estimated here can be
581 thought of as an upper bound on changes in formation rates, because mixing may account
582 for some of the changes during any adjustment period.
583 Here we have suggested that AABW formation has decreased by as much as -8.2
584 (±2.6) Sv for the period 1993–2006 relative to some previous time period, without
585 addressing the absolute values of AABW formation or when that previous time period
586 might be. How much AABW is being produced presently and how much was produced
587 in the past? While roughly 20 Sv of deep water of Southern Ocean origin has been
588 exported northward in the bottom limb of the MOC in recent decades according to CFC
589 inventories (Orsi et al. 2002) and inverse models (Ganachaud and Wunsch 2000; Sloyan
590 and Rintoul 2001; Lumpkin and Speer 2007), a more relevant formation rate estimate for
591 the classic definition of AABW (roughly $\theta < 0$°C) is 8.1–9.4 Sv from a CFC inventory
592 (Orsi et al. 1999). This inventory-based estimate is centered around 1980, and gives a
593 rough residence time of 120 years using a climatological volume for $\theta < 0$ºC (although
594 the concept of a reference time becomes complex when both the ventilation rate and
595 reservoir volume are changing). If the 8.1–9.4 Sv AABW production rate is
596 representative of earlier decades, our results would seem to imply that AABW production
597 rates have slowed to near zero during the period 1993–2006. Since measurements show

598 AABW is still being produced during these times (e.g., Gordon et al. 2001; Whitworth
599 and Orsi 2006; Williams et al. 2008) this conclusion seems unlikely.
600 It may be more reasonable to suspect that AABW production rates were already
601 lower around 1980 than in previous decades, so that earlier pure AABW formation could
602 have as much as double the CFC inventory estimate, as supported by the following two
603 arguments. First, a similar NADW formation rate estimate (LeBel et al. 2008) is twice
604 that for pure AABW, and about equal for the total contribution of Southern Hemisphere
605 waters to the bottom limb of the MOC, but these southern bottom waters fill about 1.7
606 times more of the ocean volume than NADW (Johnson 2008), suggesting that over the
607 past millennia or so AABW formation rates may have been on average larger than
608 NADW formation rates. Second, as discussed above, the SAM index has been rising at
609 least since the 1950s, and may be associated with a reduction in AABW production rates.
610 Therefore, AABW production rates may have started declining from previous larger
611 values as early as the 1950s.

612 *Acknowledgments*. We thank all those who participated in the collection of the
613 WOCE and GO-SHIP data used here. Arnold Gordon made some useful suggestions
614 regarding AABW kinematics. The comments from three anonymous reviewers greatly
615 improved the manuscript. The findings and conclusions in this article are those of the
616 authors and do not necessarily reflect the views of the National Oceanic and Atmospheric
617 Administration (NOAA). This work was supported by the NOAA Climate Program
618 Office, NOAA Research, and NASA Headquarters under the NASA Earth and Space
619 Fellowship Program - Grant NNX11AL89H.
620

620 REFERENCES

621 Aoki, S., S. R. Rintoul, S. Ushio, S. Watanabe, and N. L. Bindoff, 2005: Freshening of
622 the Adélie Land Bottom Water near 140°E. *Geophys. Res. Lett.,* **32**, L23601,
623 doi:10.1029/2005GL024246.
624 Arblaster, J. M., and G. A. Meehl, 2006: Contributions of external forcings to Southern
625 Annular Mode trends. *J. Climate*, **19**, 2896–2905.
626 Boe, J., A. Hall, and X. Qu, 2009: Deep ocean heat uptake as a major source of spread in
627 transient climate change simulations. *Geophys. Res. Lett.*, **36**, L22701,
628 doi:10.1029/2009GL040845.
629 Böning, C. W., A. Dispert, M. Visbeck, S. R. Rintoul, and F. U. Schwarzkopf, 2008: The
630 response of the Antarctic Circumpolar Current to recent climate change. *Nature*
631 *Geosci,.* **1**, 864–869.
632 Bryden, H. L., H. R. Longworth, and S. A. Cunningham, 2005: Slowing of the Atlantic
633 meridional overturning circulation at 25°N. *Nature*, **438**, 655–657,
634 doi:10.1038/nature04385.
635 Carmack, E. C., and T. D Foster, 1975: On the flow of water out of the Weddell Sea,
636 *Deep Sea Res*., **22**, 711–724.
637 Church, J. A., and Coauthors, 2011: Revisiting the Earth's sea-level and energy budgets
638 from 1961 to 2008. *Geophys. Res. Lett*., **38**, L18601, doi:10.1029/2011GL048794.
639 Clark, P., N. G. Pisias, T. F. Stocker, and A. J. Weaver, 2002: The role of the
640 thermohaline circulation in abrupt climate change. *Nature*, **415**, 863–869.

641 Coles, V. J., M. S. McCartney, D. B. Olson, and W. M. Smethie Jr., 1996: Changes in
642 Antarctic Bottom Water properties in the western South Atlantic in the late 1980s. *J.*
643 *Geophys. Res*., **101**, 8957–8970.
644 Cunningham, S. A., and Coauthors, 2007: Temporal variability of the Atlantic Meridional
645 Overturning Circulation at 26.5°C. *Science*, **317**, 935–938.
646 DeVries, T., and F. Primeau, 2011: Dynamically and observationally constrained
647 estimates of water-mass distributions and ages in the global ocean. *J. Phys.*
648 *Oceanogr.*, **41**, 2381–2401, doi:10.1175/JPO-D-10-05011.1
649 Fahrbach, E., M. Hoppema, G. Rohardt, M. Schroder, and A. Wisotzki, 2004: Decadal-
650 scale variations of water mass properties in the deep Weddell Sea. *Ocean Dynamics*,
651 **54**, 77–91.
652 Fahrbach E., M. Hoppema, G. Rohardt, O. Boebel, O. Klatt, and A. Wisotzki, 2011:
653 Warming of deep and abyssal water masses along the Greenwich meridian on decadal
654 time scales: The Weddell gyre as a beat buffer. *Deep-Sea Res. II,* **58**, 2508–2523,
655 doi:10.1016/j.dsr2.2011.06.007.
656 Foster, T. D., and Carmack, E. C., 1976: Frontal zone mixing and Antarctic Bottom
657 Water formation in the southern Weddell Sea. *Deep-Sea Res.*, **23**, 301–317.
658 Frajka-Williams, E., S. A. Cunningham, H. Bryden, and B. A. King, 2011: Variability of
659 Antarctic Bottom Water at 24.5°N in the Atlantic. *J. Geophys. Res.*, **116**, C11026,
660 doi:10.1029/2011JC007168.
661 Fukamachi, Y., S. R. Rintoul, J. A. Church, S. Aoki, S. Sokolov, M. A. Rosenberg, and
662 M. Wakatsuchi, 2010: Strong export of Antarctic Bottom Water east of the Kerguelen
663 plateu, *Nature Geosci.*, **3,** 327–331, doi:10.1038/NGE0842.

664 Fukasawa, M., H. Freeland, R. Perkin, T. Watanabe, H. Uchida, and A. Nishima, 2004:
665 Bottom water warming in the North Pacific Ocean. *Nature*, **427**, 825–827.
666 Ganachaud, A., and C. Wunsch, 2000: Improved estimates of global ocean circulation,
667 heat transport and mixing from hydrographic data. *Nature*, **408**, 453–457,
668 doi:10.1038/35044048.
669 Gille, S. T., 2002: Warming of the Southern Ocean since the 1950s. *Science*, **295**, 1275–
670 1277.
671 Gille, S. T., 2008: Decadal-scale temperature trends in the Southern Hemisphere ocean. *J.*
672 *Climate*, **21**, 4749–4765.
673 Gillett, N. P., and D. W. J. Thompson, 2003: Simulation of recent Southern Hemisphere
674 climate change. *Science*, **302**, 273–275.
675 Gordon, A. L., M. Visbeck, and B. Huber, 2001: Export of Weddell Sea Deep and
676 Bottom Water. *J. Geophys. Res.*, **106**, 9005–9017, doi:10.1029/2000JC000281.
677 Gordon, A. L., M. Visbeck, and J. C. Comiso, 2007: A possible link between the Weddell
678 Polynya and the Southern Annual Mode. *J. Climate*, **20**, 2558–2571.
679 Gouretski, V. V., and K. P. Koltermann, 2004: *WOCE Global Hydrographic*
680 *Climatology.* Berichte des bundesamtes für seeshifffahrt und hydrographie, 35, pp.
681 52+2 CD-ROMs.
682 Hellmer, H., O. Huhn, D. Gomis, and R. Timmermann, 2011: On the freshening of the
683 northwestern Weddell Sea continental shelf. *Ocean Sci.*, **7**, 305–316, doi:10.5194/os-
684 7-305-2011.
685 Hofmann, M., and M. A. Morales Maqueda, 2009: Geothermal heat flux and its influence
686 on the oceanic abyssal circulation and radiocarbon distribution, *Geophys. Res. Lett.,*

687 **36**, L03603, doi:10.1029/2008GL036078.
688 Jacobs, S. S., and J. C. Comiso, 1997: Climate variability in the Amundsen and
689 Bellingshausen seas. *J. Climate*, **10**, 697–709.
690 Jacobs, S. S., and C. F. Giulivi, 2010: Large multi-decadal salinity trends near the
691 Pacific-Antarctic Continental Margin. *J. Climate*, **23**, 4508–4524,
692 doi:10.1175/2010JCLI3284.1.
693 Jacobs, S., A. F. Amos, and P. M. Bruchhausen, 1970: Ross Sea oceanography and
694 Antarctic Bottom Water formation. *Deep-Sea Res.*, **17**, 935–962.
695 Johnson, G. C., 2008: Quantifying Antarctic Bottom Water and North Atlantic Deep
696 Water volumes. *J. Geophys. Res*., **113**, C05027, doi:10.1029/2007JC004477.
697 Johnson, G. C., and S. C. Doney, 2006: Recent western South Atlantic bottom water
698 warming. *Geophys. Res. Lett*., **33**, L14614, doi:10.1029/2006GL026769.
699 Johnson, G. C., S. Mecking, B. M. Sloyan, and S. E. Wijffels, 2007: Recent bottom water
700 warming in the Pacific Ocean. *J. Climate*, **20**, 5365–5375.
701 Johnson, G. C., S. G. Purkey, and J. L. Bullister, 2008a: Warming and freshening in the
702 abyssal southeastern Indian Ocean. *J. Climate*, **21**, 5353–5365.
703 Johnson, G. C., S. G. Purkey, and J. M Toole, 2008b: Reduced Antarctic meridional
704 overturning circulation reaches the North Atlantic Ocean. *Geophys. Res. Lett.,* **35**,
705 L22601, doi:10.1029/2008GL035619.
706 Joyce, T. M., 1991: Introduction to the collection of expert reports compiled for the WHP
707 Program. WOCE Hydrographic operations and methods. WOCE Operations Manual.
708 WHP Office Report WHPO-91-1, WOCE Report 68/91.

709 Kanzow, T., and Coauthors, 2007: Observed flow compensation associated with the
710 MOC at 26.5°N in the Atlantic. *Science*, **317** (5840), 938–941.
711 Kawano, T., M. Fukawasa, S. Kouketsu, H. Uchida, T. Doi, I. Kaneko, M. Aoyama, and
712 W. Schneider, 2006: Bottom water warming along the pathways of lower circumpolar
713 deep water in the Pacific Ocean. *Geophys. Res. Lett.*, **33**, L23613,
714 doi:10.1029/2006GL027933.
715 Kawano, T., T. Doi, H. Uchida, S. Kouketsu, M. Fukasawa, Y. Kawai, and K. Katsumata,
716 2010: Heat content change in the Pacific Ocean between the 1990s and 2000s. *Deep-*
717 *Sea Res. II,* **57**, 1141–1151, doi:10.1016/j.dsr2.2009.12.003.
718 Kirkman, C. H., IV, and C. M. Bitz, 2011: The effect of the sea ice freshwater flux on
719 Southern Ocean Temperatures in CCSM3: Deep-ocean warming and delayed surface
720 warming, *J. Climate*, **24**, 2224–2237, doi:10.1175/2010JCLI3625.1.
721 Klinger, B. A., and C. Cruz, 2009: Decadal response of global circulation to Southern
722 Ocean zonal wind stress perturbation. *J. Phys. Oceanogr.*, **39**, 1888–1904.
723 doi:10.1175/2009JPO4070.1.
724 Kouketsu, S., M. Fukasawa, I. Kaneko, T. Kawano, H. Uchida, T. Doi, M. Aoyama, and
725 K. Murakami, 2009: Changes in water properties and transports along 24°N in the
726 North Pacific between 1985 and 2005. *J. Geophys. Res.*, **114**, C01008,
727 doi:10.1029/2008JC004778.
728 Kouketsu, S., and Coauthors, 2011: Deep ocean heat content changes estimated from
729 observation and reanalysis product and their influence on sea level change. *J.*
730 *Geophys. Res.*, **116**, C03012, doi:10.1029/2010JC006464.

731 LeBel, D. A., and Coauthors, 2008: The formation rate of North Atlantic Deep Water and
732 Eighteen Degree Water calculated from CFC-11 inventories observed during WOCE.
733 *Deep-Sea Res. I,* **55**, 891–910.
734 Levitus, S., J. Antonov, and T. Boyer, 2005: Warming of the world ocean, 1955–2003.
735 *Geophys. Res. Lett.,* **32**, L02604, doi:10.1029.2004GL021592.
736 Lumpkin, R., and K. Speer, 2007, Global ocean meridional overturning. *J. Phys.*
737 *Oceanogr.,* **37**, 2550–2562.
738 Lynch-Stieglitz, J., and Coauthors, 2007: Atlantic meridional overturning circulation
739 during the last glacial maximum. *Science,* **316**, 66–69, doi:10.1126/science.1137127.
740 Mantyla, A., and J. Reid, 1995: On the origins of deep and bottom waters of the Indian
741 Ocean. *J. Geophys. Res.,* **100***,* doi:10.1029/94JC02564.
742 Masuda, S., and Coauthors, 2010: Simulated rapid warming of abyssal North Pacific
743 water. *Science*, **329**, 319–322, doi:10.1126/science.1188703.
744 Meehl, G. A., and Coauthors, 2006: Climate change projections for the Twenty-First
745 Century and climate change commitment in the CCSM3. *J. Climate*, **19**, 2597–2616.
746 doi:10.1175/JCLI3746.1.
747 Meehl, G. A., J. M. Arblaster, J. T. Fasullo, A. Hu, and K. E. Trenberth, 2011: Model-
748 based evidence of deep-ocean heat uptake during surface-temperature hiatus periods.
749 *Nature Climate Change*, **1**, 360–364, doi:10.1038/NCLIMATE1229.
750 Meredith, M. P., A. C. Naveira Garabato, A. L. Gordon, and G. C. Johnson, 2008:
751 Evolution of the deep and bottom water of the Scotia Sea, Southern Ocean, during
752 1995–2005. *J. Climate*, **21**, 3327–3343.

753 Morris, M., M. M. Hall, L. C. St. Laurent, and N. G. Hogg, 2001: Abyssal mixing in the
754 Brazil Basin. *J. Phys. Oceanogr.*, **31**, 3331–3348.
755 Oke, R. R., and M. H. England, 2004: Oceanic response to changes in the latitude of the
756 Southern Hemisphere subpolar westerly winds. *J. Climate*, **17**, 1040–1054.
757 Orsi, A. H., W. D. Nowlin Jr., and T. Whitworth III, 1993: On the circulation and
758 stratification of the Weddell Gyre. *Deep-Sea Res. I*, **40**, 169–203.
759 Orsi, A. H., T. Whitworth III, and W. D. Nowlin Jr., 1995: On the meridional extent and
760 fronts of the Antarctic Circumpolar Current. *Deep-Sea Res. I*, **42**, 641–673.
761 Orsi, A. H., G. C. Johnson, and J. L. Bullister, 1999: Circulation, mixing and production
762 of Antarctic Bottom Water. *Prog. Oceanogr.*, **43**, 55–109.
763 Orsi, A. H., W. M. Smethie Jr., and J. L. Bullister, 2002: On the total input of Antarctic
764 Waters to the deep ocean: A preliminary estimate from chlorofluorocarbon
765 measurements. *Geophys. Res. Lett.*, **107**, doi:10.1029/2001JC000976.
766 Purkey, S. G., and G. C. Johnson, 2010, Warming of global abyssal and deep Southern
767 Ocean waters between the 1990s and 2000s: Contributions to global heat and sea
768 level rise budgets. *J. Climate*, **23**, 6336–6351. doi:10.1175/2010JCLI3682.1.
769 Rignot, E., J. L. Bamber, M. R. van Den Broeke, C. Davis, Y. Li, W. Jan Van De Berg,
770 and E. van Meijgaard, 2008: Recent Antarctic ice mass loss from radar interferometry
771 and regional climate modeling. *Nature Geoscience*, **1,** 106–110,
772 doi:10.1038/ngeo102.
773 Rintoul, S. R., 2007: Rapid freshening of Antarctic Bottom Water formed in the Indian
774 and Pacific oceans. *Geophys. Res. Lett.*, **34**, L06606, doi:10.1029/2006GL028550.

775 Robertson R., M. Visbeck, A. L. Gordon, and E. Fahrbach, 2002: Long-term temperature
776 trends in the deep waters of the Weddell Sea. *Deep-Sea Res. II*, **49**, 4791–4806.
777 Roemmich, D., S. Hautala, and D. Rudnick, 1996: Northward abyssal transport through
778 the Samoan passage and adjacent regions. *J. Geophy Res.,* **101**, 14 039–14 055.
779 Russell, J. L., D. W. Dixon, A. Gnanadesikan, R. J. Stouffer, and J. R. Toggweiler, 2006:
780 The Southern Hemisphere Westerlies in a warming world: Propping open the door to
781 the deep ocean. *J. Climate*, **19**, 6382–6390.
782 Sigman, D. M., and E. A. Boyle, 2000: Glacial/interglacial variations in atmospheric
783 carbon dioxide. *Nature*, **407**, 859–869.
784 Sloyan, B. M., 2006: Antarctic bottom and lower circumpolar deep water circulation in
785 the eastern Indian Ocean. *J. Geophy. Res.*, **111**, C02006, doi:10.1029/2005JC003011.
786 Sloyan, B. M., and S. R. Rintoul, 2001: The Southern Ocean limb of the global deep
787 overturning circulation. *J. Phys. Oceanogr.*, **31**, 143–173, doi:10.1175/1520-
788 0485(2001)031<0143:TSOLOT>2.0.CO;2.
789 Smith, W. H. F., and D. R. Sandwell, 1997: Global seafloor topography from satellite
790 altimetry and ship depth sounding. *Science*, **277**, 1956–1962.
791 Solomon, S., D. Qin, M. Manning, Z. Chen, M. Marquis, K. B. Averyt, M. Tignor, and
792 H. L. Miller, Eds., 2007: Climate Change 2007: The Physical Basis. Contribution of
793 Working Group I to the Fourth Assessment Report of the Intergovernmental Panel on
794 Climate Change**,** Cambridge University Press, Cambridge, United Kingdom and New
795 York, NY, USA.
796 Stouffer, R. J., D. Seidov, and B. J. Haupt, 2007: Climate response to external sources of
797 freshwater: North Atlantic vs. the Southern Ocean. *J. Climate*, **20**, 436–448.

798 Thompson, D. W. J., S. Solomon, P. J. Kushner, M. H. England, K. M. Grise, and D. J.
799 Karoly, 2011: Signatures of the Antarctic ozone hole in Southern Hemisphere surface
800 climates change. *Nature Geoscience*, **4**, 741–749, doi:10.1038/NGEO1296.
801 Warren, B. A., and G. C. Johnson, 2002: The overflows across the Ninetyeast Ridge,
802 *Deep-Sea Res. II*, **49,** 1423–1439*,* doi:10.1016/S0967-0645(01)00156-4.
803 Whitworth, T., III, and A. H. Orsi, 2006: Antarctic Bottom Water production and export
804 by tides in the Ross Sea. *Geophys. Res. Lett.*, **33**, L12609,
805 doi:10.1029/2006GL026357.
806 Whitworth, T., III, W. D. Nowlin, R. D. Pillsbury, M. I. Moore, and R. F. Weiss, 1991:
807 Observations of the Antarctic Circumpolar Current and deep western boundary
808 current in the southwestern Atlantic. *J. Geophys. Res.*, **96**, 15 105–15 118.
809 Whitworth, T., III, B. A. Warren, W. D. Nowlin, Jr., S. B. Rutz, R. D. Pillsbury, and M. I.
810 Moore, 1999: On the deep western-boundary current in the Southwest Pacific Basin.
811 *Prog. Oceanogr.*, **43**, 1–54.
812 Williams, G. D., N. L. Bindoff, S. J. Marsland, and S. R. Rintoul, 2008: Formation and
813 export of dense shelf water from the Adélie Depression, East Antarctica. *J. Geophys.*
814 *Res.*, **113**, C04039, doi:10.1029/2007JC004346.
815 Willis, J. K., D. P. Chambers, and R. S. Nerem, 2008: Assessing the globally averaged
816 sea level budget on seasonal to interannual timescales. *J. Geophys. Res.,***113**, C06015,
817 doi:10.1029/2007JC004517.
818 Zenk, W., and E. Morozov, 2007: Decadal warming of the coldest Antarctic Bottom
819 Water flow through the Vema Channel. *Geophys. Res. Lett.*, **34**, L14607,
820 doi:10.1029/2007GJ030340.
821

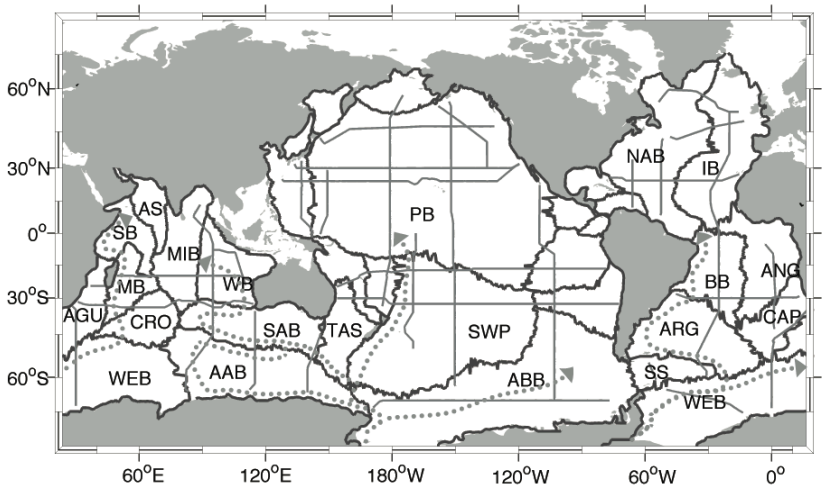

FIG. 1. Basin boundaries (thick lines), oceanographic sections (thin lines), and schematics of the four northward pathways of Antarctic Bottom Water out of the Southern Ocean (gray dotted lines). Key basins are labeled with abbreviations: Agulhas-Mozambique Basin (AGU), Crozet Basin (CRO), Madagascar Basin (MB), Somali Basin (SB), Arabian Sea (AS), Mid-Indian Basin (MIB), Wharton Basin (WB), South Australian Basin (SAB), Australian-Antarctic Basin (AAB), Tasman Sea (TAS), Pacific Basin (PB), Southwest Pacific Basin (SWP), Amundsen-Bellingshausen Basin (ABB), Scotia Sea (SS), Weddell-Enderby Basin (WEB), Argentine Basin (ARG), Brazil Basin (BB), North Atlantic Basin (NAB), Iberian/Canary/Cape Verde Basin (IB), Angola Basin (AB), and Cape Basin (CAP).

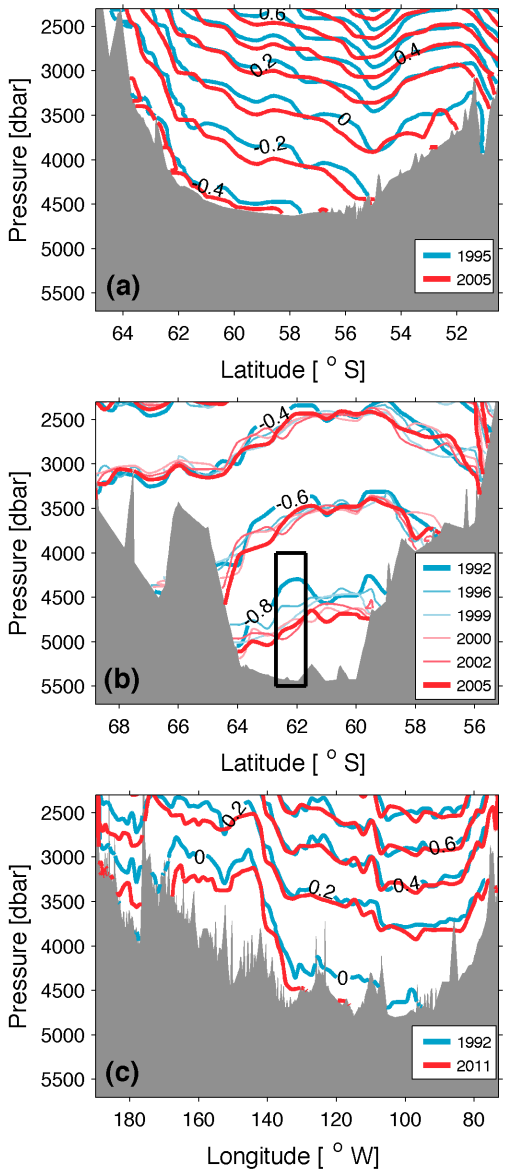

FIG. 2. Vertical-lateral profiles of select potential isotherms for each occupation of a) I09 across the Australian-Antarctic Basin, b) A12 across the Weddell-Enderby Basin, and c) S4P across the Amundsen-Bellingshausen Basin (Figs. 1 and 6). Contours of the earliest occupations are labeled and bottom topography (Smith and Sandwell 1997) is shaded gray. The black box in b is discussed in Fig. 3.

840

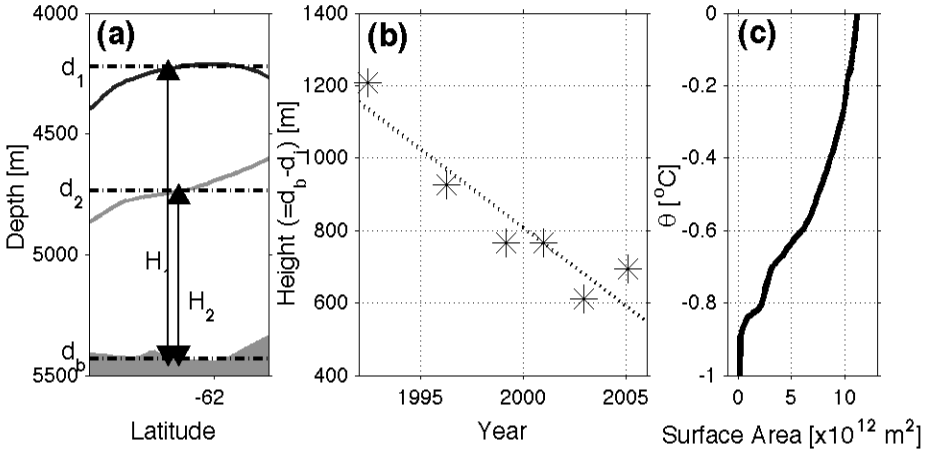

841

842 FIG. 3. Illustration of a sample volume contraction calculation taken from A12 in the
843 Weddell-Enderby Basin at 62.2°S. a) Detail of black box in Fig. 2b. Only the depth and
844 thickness for the 1992 (dark gray line and H_1) and 2005 (light gray line and H_2) -0.8°C
845 potential isotherm are shown with bottom topography (Smith and Sandwell 1997) shaded
846 gray. b) Height of θ = -0.8°C above the bottom (H) at 62.2°S during each occupation
847 (asterisks) with a least-squares linear fit (dotted line). c) Surface area of each given θ in
848 the Weddell-Enderby Basin estimated from a climatology (Gouretski and Kolterman
849 2004).

850

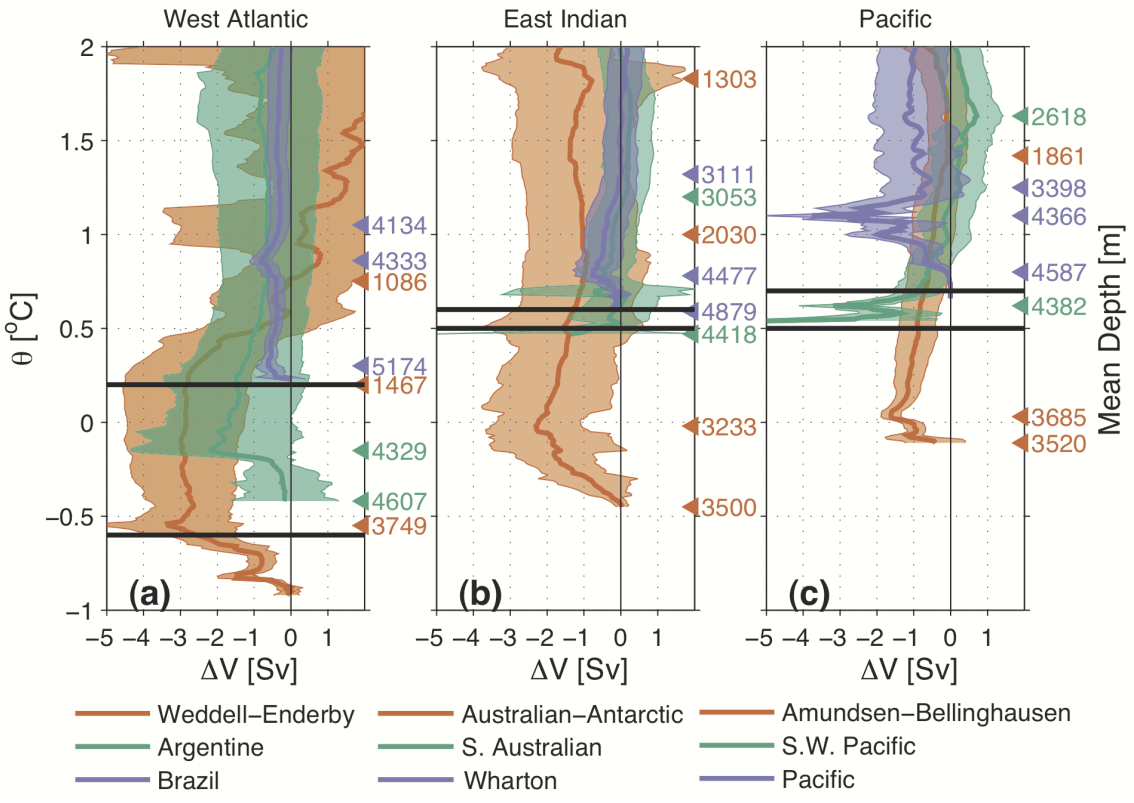

FIG. 4. Total rates of volume change for select basins (legends) below each potential isotherm (ΔV curves, solid lines) with 95% confidence intervals (shading) along three of the four northward pathways for AABW out of the Southern Ocean from south to north (orange through green to purple). Minimum θ values spreading from the orange to the green basins (lower horizontal black lines) and the green to the purple basins (upper horizontal black lines) are estimated from a climatology (Gouretski and Kolterman 2004). Color-coded numbers along the right axis indicate mean depths of selected θs for the corresponding basin.

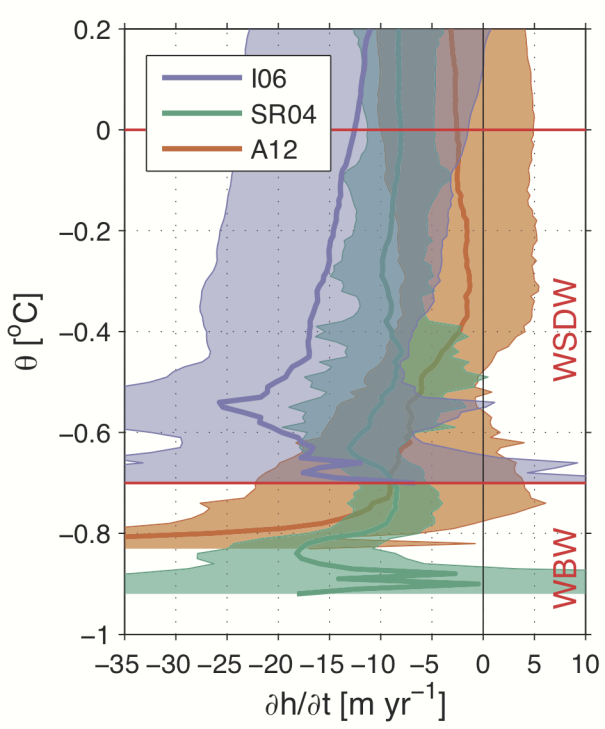

FIG. 5. Mean time rate of change in height above the bottom for potential isotherms along three repeat hydrographic sections across the Weddell-Enderby Basin (solid lines; legend; see Fig. 6 for locations) with 95% confidence intervals (shaded). Horizontal red lines indicate classically defined (Carmack and Foster 1975) limits of WSBW (θ < -0.7°C) and WSDW (-0.7 < θ < 0°C).

867

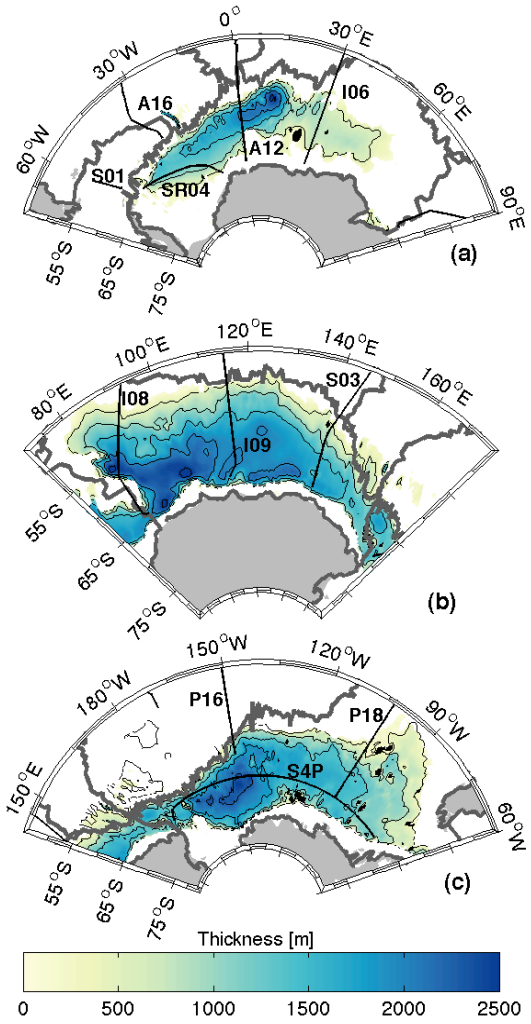

868

869 FIG. 6. Thickness (color contours) below select climatological (Gouretski and Kolterman
870 2004) potential isotherms contained in the southern basins: a) θ = -0.6°C isotherm in the
871 Weddell-Enderby Basin, b) θ = 0.4°C isotherm in the Australian-Antarctic Basin, and c)
872 θ = 0.4°C isotherm in the Amundsen-Bellingshausen Basin. Basin boundaries (thick gray
873 lines), land (shaded gray), and repeat oceanographic sections (black lines) with their
874 WOCE designators are plotted.

875

875

Basin, θ_{top}	Steady State			
	$\sum_i U_i \cdot \theta_i + W\theta_{top}$	$\kappa\theta_z \cdot SA$	$\frac{Q \cdot SA}{\rho C_p}$	$\sum_{\theta}^{\theta_{top}} (\theta_{top} - \theta) \cdot \frac{\partial \Delta V}{\partial \theta}$
Pacific Basin, 1 °C	-2.57	2.38	0.19	-0.15
Brazil Basin, 0.8 °C	-3.11	3.05	0.06	-0.25

876 TABLE 1. Heat budget terms (in Sv °C) compared to the observed imbalances for two
877 deep basins. From left to right, the advective term is the sum of all cold water volume
878 transports (U_i) through passages i into or out of the basin each with transport-weighted
879 potential temperatures (θ_i) below a top bounding potential isotherm (θ_{top}). Upwelling
880 transport through that top surface (W) is derived assuming volume conservation. Values
881 for U_i and θ_i are from Morris et al. (2001) in the Brazil Basin and Roemmich et al. (1996)
882 in the Pacific Basin. The vertical diffusion term at θ_{top} is the product of the vertical
883 diffusivity coefficient (κ), the vertical temperature gradient (θ_z), and surface area (SA) and
884 is estimated from the residual of the other two steady-state terms. For the geothermal
885 heating term, Q = 0.05 W m^{-2}, an average deep ocean value (Hofmann and Morales
886 Maqueda 2009), is applied over SA, appropriately scaled by density (ρ) and heat capacity
887 (C_p). Climatological maps (Gouretski and Koltermann 2004) are used to estimate θ_z, SA,
888 ρ, and C_p for each basin. The imbalance term (rightmost column) is determined by
889 summing the product of $\partial\Delta V/\partial\theta$ and θ_{top} - θ from the coldest waters in the basin to θ_{top}
890 (see text for further explanation).
891

891

Basin	Volume Change [Sv]
Weddell-Enderby	-2.85 (±1.59)
Australian-Antarctic	-2.24 (±1.14)
Amundsen-Bellingshausen	-1.09 (±0.28)
Argentine	-1.67 (±1.70)
Scotia Sea	-0.23 (±1.10)
Agulhas-Mozambique	-0.16 (±0.33)
Sum	-8.2 (±2.6)

892 TABLE 2. Rate of volume change below $\theta = 0$°C with 95% confidence intervals (in
893 parentheses) for the six basins containing water this cold (see Fig. 4), and their sum.